Discovery and characterization of a new class of NAD$^+$-independent SIRT1 activatorsRunning title: A novel class of STACs

S Della Torre, G Dell'Omo, J Dellavedova, L Palazzolo, E Scanziani, Eberini, A Pinto, N Mitro, P Conti, A Villa, P Ciana

PII: S1043-6618(24)00241-X

DOI: https://doi.org/10.1016/j.phrs.2024.107296

Reference: YPHRS107296

To appear in: *Pharmacological Research*

Received date: 28 February 2024
Revised date: 22 June 2024
Accepted date: 3 July 2024

Please cite this article as: S Della Torre, G Dell'Omo, J Dellavedova, L Palazzolo, E Scanziani, Eberini, A Pinto, N Mitro, P Conti, A Villa and P Ciana, Discovery and characterization of a new class of NAD$^+$-independent SIRT1 activatorsRunning title: A novel class of STACs, *Pharmacological Research,* (2024) doi:https://doi.org/10.1016/j.phrs.2024.107296

Title: **Discovery and characterization of a new class of NAD$^+$-independent SIRT1 activators**

Authors: Della Torre S[1], Dell'Omo G[2], Dellavedova J[2], Palazzolo L[3], Scanziani E[4], Eberini I[3], Pinto A[5], Mitro N[3,6], Conti P [1], Villa A[2] and Ciana P[2,*]

Affiliation:

1. Department of Pharmaceutical Sciences, Università degli Studi di Milano, Milan, Italy;
2. Department of Health Sciences, Università degli Studi di Milano, Milan, Italy;
3. Department of Pharmacological and Biomolecular Sciences "Rodolfo Paoletti", Università degli Studi di Milano, Milan, Italy;
4. Department of Veterinary Medicine and Animal Sciences, Università degli Studi di Milano Milan, Italy;
5. Department of Food, Environmental and Nutritional Sciences, Università degli Studi di Milano, Milan, Italy;
6. Department of Experimental Oncology, IEO, European Institute of Oncology IRCCS, Milan, Italy.

***Corresponding Author**: Paolo Ciana, paolo.ciana@unimi.it

Address: Department of Health Sciences, Università degli Studi di Milano, Via Antonio di Rudinì 8, 20142, Milan, Italy.

Running title: A novel class of STACs

Keywords: sirtuin-activating compounds; NAD$^+$-dependent deacetylases, sulindac analogues, ageing-associated diseases, metabolic diseases

Abstract

The activity of sirtuin 1 (SIRT1, a member of the NAD^+-dependent deacetylases family) decreases during aging as NAD^+ levels naturally decline, thus increasing the risk of several age-associated diseases. Several sirtuin-activating compounds (STACs) have been developed to counteract the age-associated reduction in SIRT1 activity, and some of them are currently under development in clinical trials. STACs induce SIRT1 activation, either through allosteric activation of the enzyme in the presence of NAD^+, or by increasing NAD^+ levels by inhibiting its degradation or by supplying a key precursor in biosynthesis. In this study, we have identified (*E*)-2'-des-methyl sulindac analogues as a novel class of STACs that act also in the absence of NAD^+, a peculiar behavior demonstrated through enzymatic and mass spectrometry experiments, both *in vitro* and in cell lines. The activation of the SIRT1 pathway was confirmed *in vivo* through gene expression and metabolomics analysis. Our data suggest that these compounds could serve as candidate leads for a novel therapeutic strategy aimed at addressing a key metabolic deficiency that may contribute to metabolic and age-associated diseases.

Introduction

The increasing incidence of metabolic diseases, such as metabolic syndrome (MS), obesity, insulin resistance (IR), type 2 diabetes mellitus (T2DM), metabolic dysfunction-associated steatotic liver disease (MASLD), and cardiovascular diseases (CVDs), reflects changes in dietary habits and lifestyles [1], as well as the growing aging population observed worldwide [2]. Indeed, the aging-related decline of cell and tissue functions impacts the regulatory processes of glucose and lipid metabolism, favoring the onset and development of many chronic metabolic diseases [3].

Although the inverse relationship has been less investigated [4], altered metabolism and chronic metabolic diseases might promote the development of a chronic inflammatory status, thus

contributing to the progression of aging-related phenotypes [5]. The bidirectional relationship between aging and metabolic diseases underscores shared molecular and cellular mechanisms [5,6] that might allow for the identification of key drivers and potential common pharmacological targets. Among these, the mammalian sirtuin family has gained significant interest due to its relevance in physiology and its role in promoting stress responses and longevity, as well as in delaying aging and age-related diseases [7–9].

In mammals, there are seven sirtuin homologs (SIRT1-7), differing in their expression, subcellular localization (nuclear: SIRT1, SIRT6, and SIRT7; mitochondrial: SIRT3, SIRT4, and SIRT5; cytosolic: SIRT2, mechanism of action, and binding partners and substrates [10]. Sirtuins catalyze NAD^+-dependent deacetylation [11] through a two-step reaction involving the consumption of NAD^+ and the acetylated protein substrate to produce nicotinamide (NAM), 2' O-acetyl-adenosine diphosphate-ribose (O-AcADPR), and deacetylated substrate. In the first step, NAD^+ is cleaved, accompanied by the release of free NAM, and ADP-ribose is covalently attached to the acetyl moiety of the substrate; in the second step, the hydrolysis of the acetyl-lysine bond occurs, liberating O-AcADPR [12].

To date, the sirtuin that has received the most attention as a drug target for its potential metabolic health benefits is SIRT1 [13,14]. By deacetylating key histone residues involved in the regulation of transcription and several non-histone protein targets (including p53, FOXO1/3, PGC-1α, and NF-κB), SIRT1 can regulate several metabolic signaling pathways, including glucose and insulin homeostasis, mitochondrial biogenesis, circadian rhythms, muscle and fat differentiation [10].

Due to the health benefits observed in mice with SIRT1 over-expression, developing pharmacological approaches aimed at increasing the enzymatic activity of SIRT1 became a major goal in the field [15,16]. With a better molecular understanding of sirtuin structure and catalysis [17,18], and through high-throughput screening, significant efforts have been directed towards developing sirtuin-activating compounds (STACs). Although STACs increase SIRT1 activity across multiple substrates, resulting in various biological responses [15,19], their molecular mechanism remains controversial [20,21].

Skepticism regarding direct activation of SIRT1 by STACs has been raised in some studies [22], although strong evidence of allosteric activation for molecules targeting the N-terminal portion of SIRT1 has been produced [17,19,23]. Another class of STACs consists of NAD^+-boosting molecules that target biosynthetic enzymes or provide precursor metabolites to increase intracellular NAD^+ levels, thus potentially activating all sirtuins [24]. None of the STACs identified so far have been shown to act as NAD^+-independent activators, behaving as acetyl acceptors in the deacetylases reaction; these compounds would directly activate SIRT1, decoupling the enzymatic modulation from endogenous NAD^+ levels, making this class of molecules particularly attractive for replacement therapy in individuals with low NAD^+ levels, such as the elderly and individuals with chronic illnesses like metabolic diseases, heart disease, neurodegenerative, and neurological disorders.

In our previous research, we demonstrated that exisulind – a sulfone metabolite of the nonsteroidal anti-inflammatory drug sulindac – could compete with NAD^+ for binding to the catalytic pocket of SIRT1 and inhibit enzymatic activity by blocking access to the channel of the acetylated lysine substrate [25]. In the present study, different (*E*)-2'-des-methyl sulindac analogues were tested for their potential roles as SIRT1 inhibitors or activators. Here, we identify two (*E*)-2'-des-methyl sulindac analogues that retain the ability to bind the catalytic pocket and activate SIRT1 in a NAD^+-independent way, thus defining a novel class of STACs.

RESULTS

Compound selection for the study

In order to identify selective SIRT1 modulators among different variants of the exisulind scaffold, we opted to begin with molecules demonstrating low or negligible COX-1/2 activity. The research group led by J. Marnett revealed that the 2'-methyl group of sulindac sulfide, the active metabolite of sulindac, plays a crucial role in tight binding to COX-1 and COX-2, as is the case with indomethacin

[26,27]. Interestingly, while sulindac sulfide is a potent time-dependent COX-1/2 inhibitor (IC_{50} = 115 nM for COX-1, IC_{50} = 140 nM for COX-2), (*E*)-2'-des-methyl sulindac sulfide is a very weak, rapid, and reversible COX-1 inhibitor (IC_{50} = 1.8 μM for COX-1) and has no inhibitory effect on COX-2 (IC_{50} > 4 μM for COX-2). Based on this data, we chose to shift our focus from sulindac derivatives to analogues of (*E*)-2'-des-methyl sulindac, aiming to select compounds with reduced COX inhibitory activity. As previously documented, such compounds serve as valuable tools to elucidate the non-COX-mediated biological functions of NSAIDs [28,29].

An extensive structure-activity relationship (SAR) study centered around the (*E*)-2'-des-methyl sulindac scaffold had previously been reported [26,29], resulting in the synthesis and characterization of multiple analogs for their COX inhibitory activity. Among these, we have chosen four compounds for our investigation, all exhibiting weak or negligible COX-1 inhibitory activity and no COX-2 inhibitory activity. Specifically, we chose a compound featuring an electron-donor group in the para position of the aromatic ring (R = tBuO, compound RB2), one with an electron-withdrawing group (R = SO_2CH_3, compound RB12), and two compounds characterized by the presence of a bulky and lipophilic substituent, namely the biphenyl derivative RB4 and the 1-naphthyl derivative RB7 (see Supplementary Fig. 1).

(*E*)-2'-Des-methyl sulindac -derivatives act as NAD^+-independent SIRT1 activators

The activity of (*E*)-2'-des-methyl sulindac derivatives as potential SIRT1 inhibitors or activators was initially tested by using an *in vitro* assay that measures the fluorescence produced by a two-step reaction initiated by the acetyl removal from a fluorescent-substrate peptide containing an acetylated lysine followed by the cleavage of the substrate and the release of a highly fluorescent residue.

While RB2 and RB12 acted as SIRT1 inhibitors (Supplementary Fig. 2), RB4 and RB7 showed the opposite activity with a trend to increase SIRT1 activation at high doses (Fig. 1A-C). In keeping with these results, RB4 and RB7 increased the activity of native SIRT1 present in protein extracts from

MDA-MB-231 cells in a dose-dependent manner (Fig. 1D-F). RB2 and RB12 behaved like exisulind and, although interesting from a drug discovery perspective, were not considered novel from a mechanistic standpoint[25]. Therefore, we decided to set them aside and concentrate on the activators.

Due to the limitation of the SIRT1 fluorescence-based assay [22,30], we further tested the RB4 and RB7 activity by evaluating the changes in p53 acetylation of native p53 [25], a well-known target of the deacetylase [10]. The content of p53 isoforms (total and acetylated at the K382 residue) was therefore measured by western blot of the protein extracts from MDA-MB-231 cells treated with 270 μM of exisulind, RB4 and RB7 for 3 hours. Etoposide (20 μM) was also included in the study as a control since this drug acts as a potent and specific small-molecule inhibitor of SIRT1 catalytic activity [31]. As shown in Fig. 1G, differently from exisulind and etoposide, RB4 and RB7 slightly decreased the low baseline level, instead of increasing the acetylation of p53, thus supporting the notion that their effects were directly mediated by SIRT1. To further strengthen this conclusion, we evaluated the RB4 potential ability of interfering with the SIRT1-mediated increase of p53 acetylation in MDA-MB-231 cells treated with etoposide. After 3 hours of treatment, increasing concentrations of RB4 (30-90-270 μM) significantly decreased the etoposide-induced acetylation of p53 (Fig. 1H), thereby confirming the activating role of this compound. We then investigated whether the effect of RB4 and RB7 on p53 acetylation was mediated by SIRT1 in cells. To this end, we treated HEK293 wild type and HEK293 SIRT1 KO cells with etoposide and increasing concentrations of RB4 and RB7. The results clearly demonstrated that RB4 was able to decrease p53 acetylation only in wild type cells and not in KO cells (Supplementary Fig. 3). Moreover, these experiments showed that RB7 had a limited ability to counteract etoposide-mediated p53 acetylation compared to RB4 (Supplementary Fig. 3).

Our previous docking results indicated that exisulind binds to a region of the enzyme that overlaps with the NAD^+ binding site[25], thereby suggesting that the mechanism of activation of the exisulind derivatives could be independent of the presence of the co-factor. To test this hypothesis, we measured changes in SIRT1 activity induced by these compounds in the absence of NAD^+. The results clearly

demonstrated that both RB4 and RB7 retained their ability to activate SIRT1 even under these conditions (Fig. 1I-M), implying that NAD^+ was not necessary for their mechanism of action. These findings prompted us to hypothesize that these compounds might emulate NAD^+, despite the absence of an evident correlation between the chemical structure of RB4 and RB7 and the enzyme's co-factor.

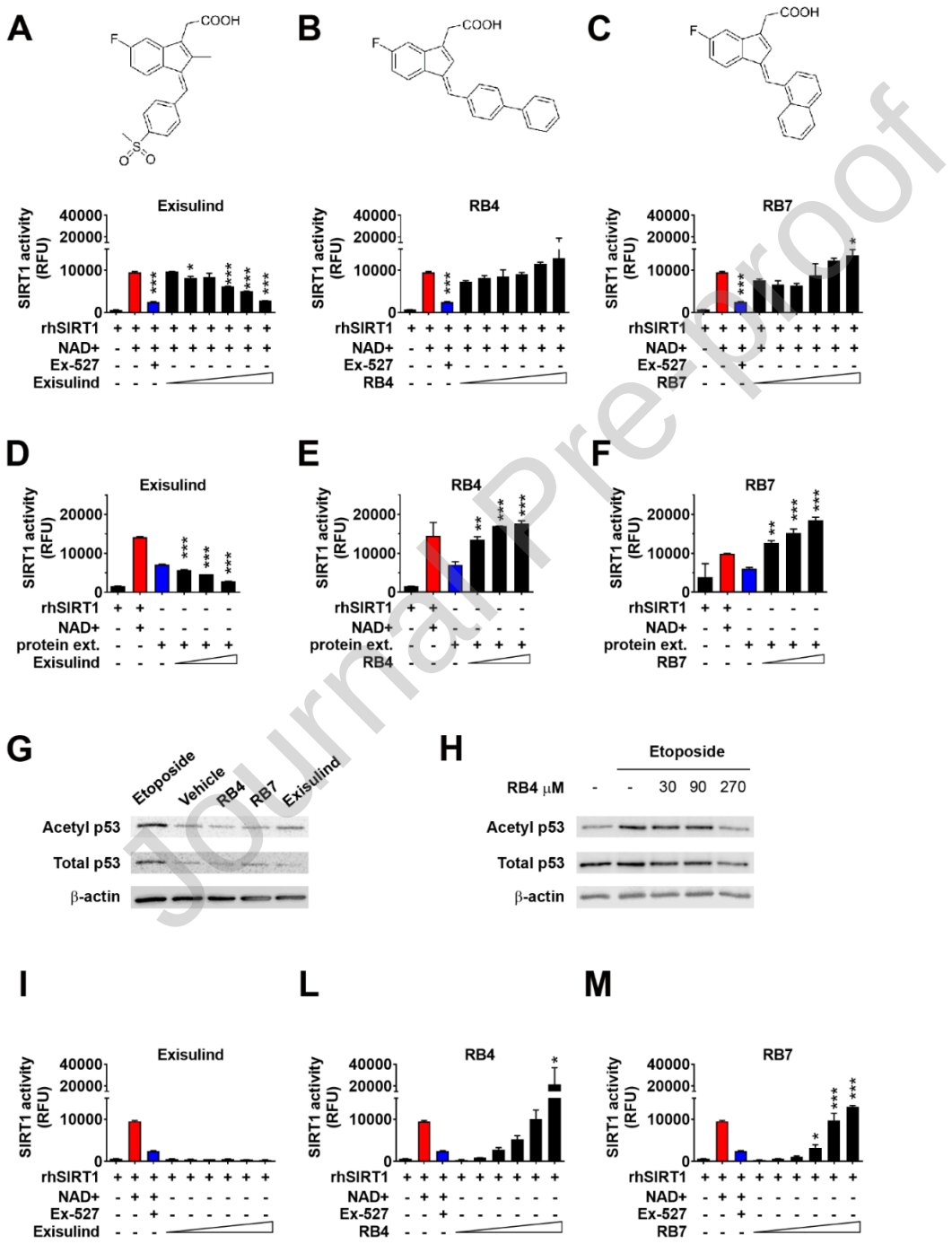

Figure 1: Exisulind derivatives increase SIRT1 activity *in vitro*, even in the absence of NAD^+. A-C. rhSIRT1 activity was measured *in vitro* with a fluorescence-based assay in the presence of 200 μM β-

nicotinamide adenosine dinucleotide (NAD^+) and of increasing concentrations (11, 33, 100, 300, 900, 2700 μM) of Exisulind (**A**), RB4 (**B**) or RB7 (**C**); treatment with 10 μM EX-527, a selective inhibitor of rhSIRT1, was used as positive control of the reactions. Data are represented as mean ± SEM. *p<0.05, **p<0.01 and ***p<0.001 *vs* the value of the NAD^+ treated sample (the red bar) by one-way ANOVA followed by Bonferroni's *post hoc* test. **D-F**. The sirtuin activity was tested in MDA-MB-231 protein extracts treated with increasing concentrations (300, 900, 2700 μM) of Exisulind (**D**), RB4 (**E**) or RB7 (**F**). Data are represented as mean ± SEM. *p<0.05, **p<0.01 and ***p<0.001 *vs* the value of the vehicle treated sample (the blue bar) by one-way ANOVA followed by Bonferroni's *post hoc* test. **G**. Pictures show a representative immunoblot analysis of native acetylated (K382) and total p53 present in protein extracts obtained from MDA-MB-231 cells after 3 h treatment with Etoposide (20 μM), vehicle (DMSO), RB4 (90 μM), RB7 (90 μM), and Exisulind (90 μM). β-actin is reported as loading control. **H**. Pictures show a representative immunoblot analysis of native acetylated and total p53 present in protein extracts obtained from MDA-MB-231 cells after 3 h treatment with/without Etoposide (20 μM) and increasing concentration of RB4 (30, 90, 270 μM). B-actin is reported as loading control. **I-M**. rhSIRT1 activity was measured *in vitro* with a fluorescence-based assay in the presence of increasing concentrations (11, 33, 100, 300, 900, 2700 μM) of Exisulind (**I**), RB4 (**L**) or RB7 (**M**) and in the absence of NAD^+; treatment with 10 μM EX-527 was used as positive control of the reactions. Data are represented as mean ± SEM. *p<0.05, **p<0.01 and ***p<0.001 *vs* the value of the vehicle treated sample (the first bar) by one-way ANOVA followed by Bonferroni's *post hoc* test.

Insights into the mechanism of action of a novel class of NAD^+-independent SIRT1 activators

To test the hypothesis of RB4's NAD^+-mimetic activity with a potential role as an acetyl acceptor, we conducted mass spectrometry analyses to characterize the reaction products. Initially, we analyzed the SIRT1 enzymatic assay solution. In the absence of SIRT1 in the reaction mixture (Fig. 2A and B), we only detected the m/z 311 ion, which represented the decarboxylated form of RB4 (Supplementary Fig. 4). However, upon adding SIRT1 to the *in vitro* assay, we observed the appearance of the m/z 413 parent ion (Fig. 2C) that could derive from the addition of a carboxymethyl radical to RB4 (+58). Collision of the m/z 413 ion generated a transition at m/z 369, due to decarboxylation (−44), an ion at m/z 355 corresponding to RB4's molecular weight ($[M-H]^-$) and an ion at m/z 311, which represented the decarboxylated form of RB4 (Fig. 2D). Similar results were obtained with RB7 molecule (Supplementary Fig. 5).

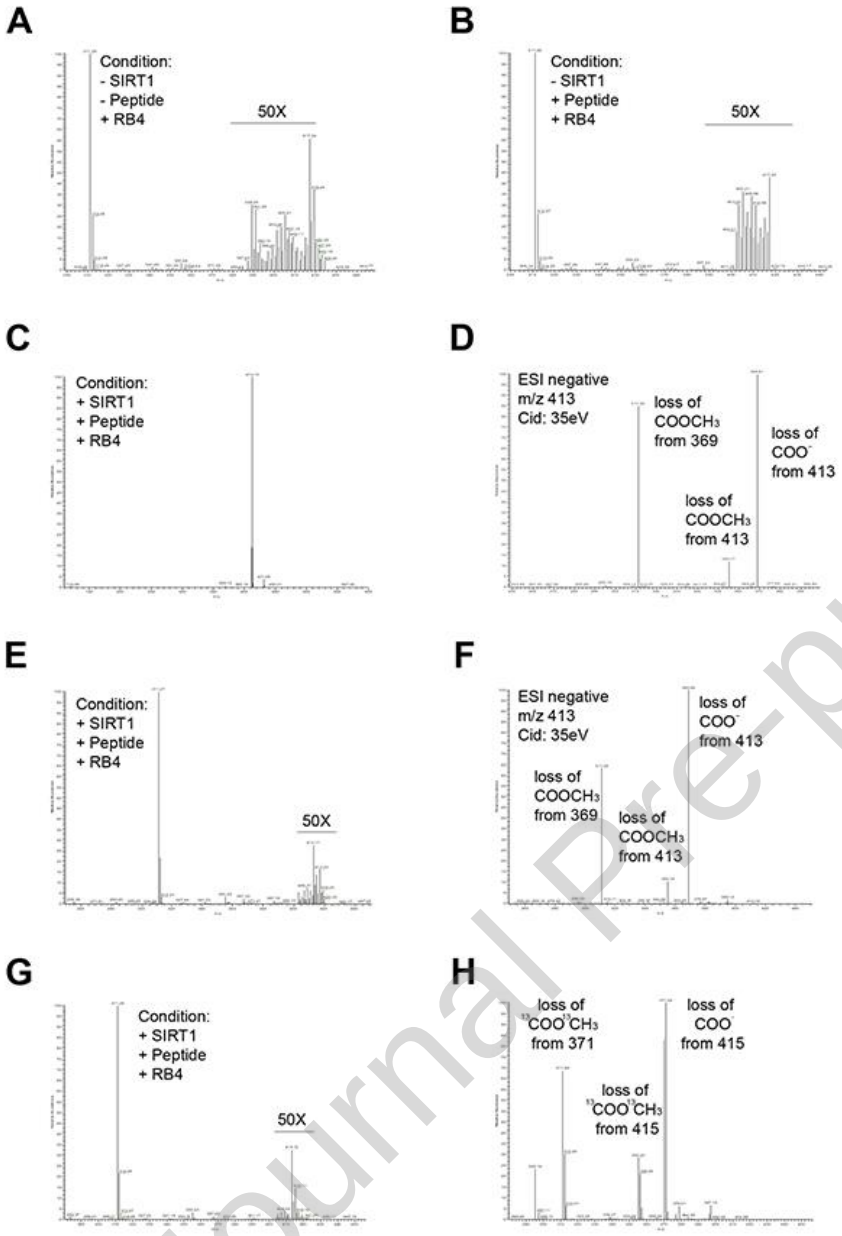

Figure 2: Detection and fragmentation pattern of the m/z 413 ion obtained by negative ion mode ESI-IT-MS/MS. A-B. Spectra showing the absence of acetylated RB4 when SIRT1 is not present in the reaction mixture of the enzymatic *in vitro* assay. m/z 311 represents the diagnostic ion of unmodified RB4. **C-D**. Detection (**C**) and fragmentation pattern (**D**) of the m/z 413 ion corresponding to the acetylated form of RB4 in enzymatic *in vitro* assay. Specific losses and energy used to induce fragmentation (collision-induced dissociation, Cid) are indicated. **E-F**. Detection (**C**) and the m/z 413 ion (**F**) corresponding to the acetylated form of RB4 in MDA-MB-231 cell lysate. **G-H**. Detection (**G**) and the m/z 415 ion (**H**) corresponding to the labeled acetylated form of RB4 in MDA-MB-231 cell lysate previously exposed to [U-$^{13}C_2$]-acetate. Specific losses are indicated, and Cid was 35eV. 50X represents the spectrum magnification in the indicated regions.

We then sought to determine if these findings could be replicated in a cellular system, focusing only on RB4, as RB7 proved less effective in the cellular system (Supplementary Fig. 3). As shown in Fig. 2E and 2F, RB4 exhibited the same m/z 413 parent ion observed in the *in vitro* assay, along with the same fragmentation pattern. We also exposed MDA-MB-231 cells to [U-$^{13}C_2$]-acetate. Alongside the m/z 413 parent ion, we detected the m/z 415 labeled molecular ion (Fig. 2G), suggesting an addition of the ^{13}C-labelled radical fragment on the molecule of RB4. Fragmentation analysis of the m/z 415 ion displayed a pattern consistent with that observed before (Fig. 2H).

To investigate the potential interaction sites between RB4, RB7, and SIRT1, we conducted meticulous molecular docking analysis. In Fig. 3A, we present the highest-scoring binding poses of RB4 and RB7 in green and violet, respectively. Both compounds demonstrated efficient binding to the NAD^+ binding site, suggesting a likely competitive binding (Fig. 3B). The indenacetic group of these compounds perfectly overlapped in the top-scoring binding poses. The approximate binding free energies, computed using empirical scoring functions (please refer to the Methods and Materials section), were negative (RB4: -7.3 kcal/mol; RB7: -6.9 kcal/mol), implying their potential to bind to SIRT1, albeit lower than the reference co-crystallized SIRT1 inhibitor (-9.1 kcal/mol). Fig. 3C shows SIRT1 (PDB ID 4ZZI) bound to the small molecule sirtuin-activating compounds (STAC), in yellow, and to the acetylated peptide substrate of SIRT1, in orange, both transferred from the PDB file 4ZZJ. Notably, the acetyl-lysine of the substrate significantly bumps with both the biphenyl group of RB4 and the 1-naphthyl group of RB7. Thus, although the docking results suggest the binding of RB4 and RB7 in the NAD^+ pocket of SIRT1, these data do not offer a clear indication of the biochemical mechanism by which the two molecules take part in the enzymatic reaction (Fig. 2).

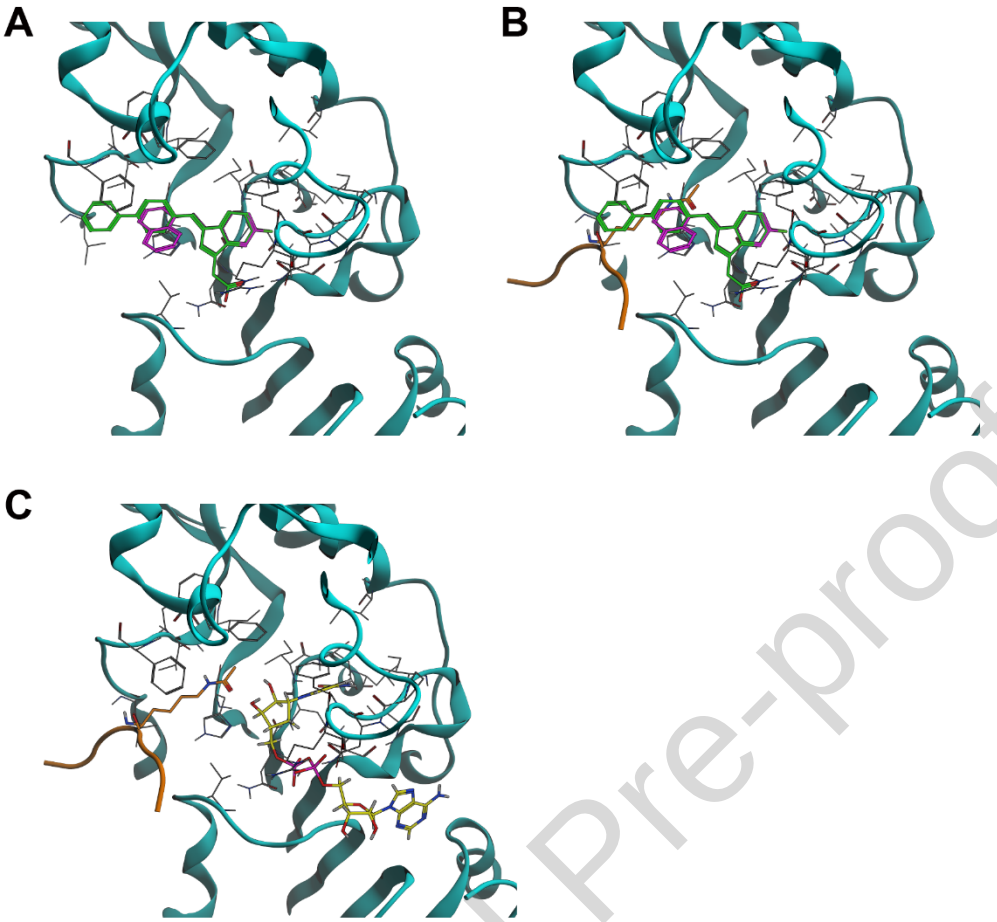

Figure 3: Highest-scoring binding poses of RB4 and RB7. A, **B**. Highest-scoring binding poses of RB4 (green) and RB7 (violet) (**A**), and in presence (**B**) of acetylated peptide substrate (orange) of SIRT1 (light blue ribbon), transferred from PDB ID: 4ZZJ. **C**. SIRT1 (light blue ribbon) bound to the acetylated peptide substrate (orange) and to the small molecule sirtuin-activating compounds (STAC) (yellow).

Physiological relevance of RB4 as an *in vivo* SIRT1 activator

Given the main effects of RB4 in cell-based experiments, we therefore decide to assess RB4's capacity to serve as a SIRT1 activator and modulate SIRT1-dependent signaling *in vivo*. We thus administered RB4 orally to male mice at two doses (5 and 50 mg/kg/day) over a 3-day period (Supplementary Fig. 6A). Throughout the experiment, we monitored changes in body weight and food intake, observing no significant differences in comparison to the control group treated with the vehicle (Supplementary Fig. 6 B-C). After the 3-day treatment period, we euthanized the mice in the

early afternoon following a 6-hour fast, and excised liver samples were subjected to histological and biochemical analyses.

No lesions of evident toxicological significance were observed in the livers of RB4-treated mice, indicating the absence of liver toxicity induced by this treatment (Supplementary Fig. 6D). Minimal hypertrophy of centrilobular hepatocytes, related to microsomal enzyme induction, was observed in only one mouse from the high-dose group. Infiltrates of inflammatory cells (lymphocytes, granulocytes, macrophages) were detected in 3 out of 5 mice in the control group and 1 out of 10 in the treated groups, suggesting a potential anti-inflammatory action of this compound (Supplementary Fig. 6D). The analysis of mRNA levels of various Nuclear factor-kB (NF-kB) target genes confirmed this anti-inflammatory activity. It is known that SIRT1-mediated deacetylation negatively regulates NF-kB [10] (Fig. 4A). Accordingly, the majority of NF-kB target genes were dose-dependently inhibited by RB4 (Fig. 4B), suggesting that SIRT1 activation through a NAD^+-independent mechanism effectively suppressed the pro-inflammatory signaling pathway in the liver.

Further gene expression analysis focused on established SIRT1 targets involved in liver metabolism regulation [32,33]. Upon activation, SIRT1 interacts with and deacetylates PGC1α (peroxisome proliferative activated receptor, gamma, coactivator 1 alpha), thereby promoting gluconeogenic gene transcription in the liver [32] (Fig. 4C). RB4 treatment induced mRNA levels of *Pgc1α*, as well as those of *Pck1* (phosphoenolpyruvate carboxykinase 1) and *G6pc* (glucose-6-phosphatase), two crucial genes involved in gluconeogenesis (GNG). Correspondingly, a repression of the glycolytic gene *Gck* (glucokinase) was observed (Fig. 4D).

To comprehensively understand the physiological implications of the observed changes, we quantitatively measured the most relevant metabolites in the liver. In line with gene expression data, the heatmap of liver metabolites (Supplementary Fig. 7 and Supplementary Table 2) highlighted significant metabolic effects in the RB4-treated groups, as further emphasized by Principal Component Analysis (PCA) (Fig. 4E). Notably, some gluconeogenic amino acids (Ala, Gln, His) exhibited a decreasing trend (Fig. 4F), while intermediates of GNG (glucose-6-phosphate, G6P, and

dihydroxyacetone phosphate/glyceraldehyde 3-phosphate, DHAP/GAP) displayed an increasing trend, alongside a substantial rise in malate (a TCA cycle-derived GNG precursor) (Fig. 4G). These changes were consistent with alterations in *Pck1* and *G6pc* mRNA, further supporting the notion of SIRT1-mediated GNG stimulation induced by RB4.

Upon activation, SIRT1 deacetylates and promotes the degradation of SREBP1 (sterol regulatory element-binding protein 1) through the ubiquitin–proteasome system, thereby suppressing lipid synthesis [32,34] (Fig. 4H). To investigate the modulation of lipogenesis, we examined the expression of SREBP1 target genes involved in fatty acid (*Acaca*, acetyl-CoA carboxylase alpha; *Fasn*, fatty acid synthase) and triglyceride (*Dgat2*, diacylglycerol O-acyltransferase 2) synthesis. As depicted in Fig. 4I, RB4 dose-dependently decreased the expression of these genes, consistent with the expected outcomes of SIRT1 activation. Furthermore, several studies have indicated that SIRT1-dependent regulation of lipogenic enzymes occurs through the induction of FGF21 (fibroblast growth factor 21) [35]. As per this report, RB4 treatment elevated hepatic *Fgf21* expression (Fig. 4I).

SIRT1's extensive impact on the liver also encompasses the modulation of genes involved in circadian regulation [36] (Fig. 4L). Aligning with the considered time window (mice were sacrificed at 2:00 pm; ZT7), we observed significant shifts in the expression of clock genes such as *Per2* (period circadian clock 2), *Cry1* (cryptochrome 1), *Cry2* (cryptochrome 2), and *Nr1d1* (nuclear receptor subfamily 1 group D member 1, also known as Rev-Erbα) due to RB4 treatment (Fig. 4M). Changes in clock gene regulation correlated with the upregulation of *Nampt* (nicotinamide phosphoribosyltransferase) (Fig. 4M), affirming the reciprocal interplay between cellular metabolism and circadian rhythms through the SIRT1 pathway [36,37]. Reflecting NAMPT's role in intracellular NAD^+ pool regulation [38], hepatic NAD^+ content exhibited an increasing trend (Fig. 4N), potentially further enhancing SIRT1 activation.

Taken together, these findings provide compelling *in vivo* evidence for RB4's SIRT1 activation observed *in vitro*.

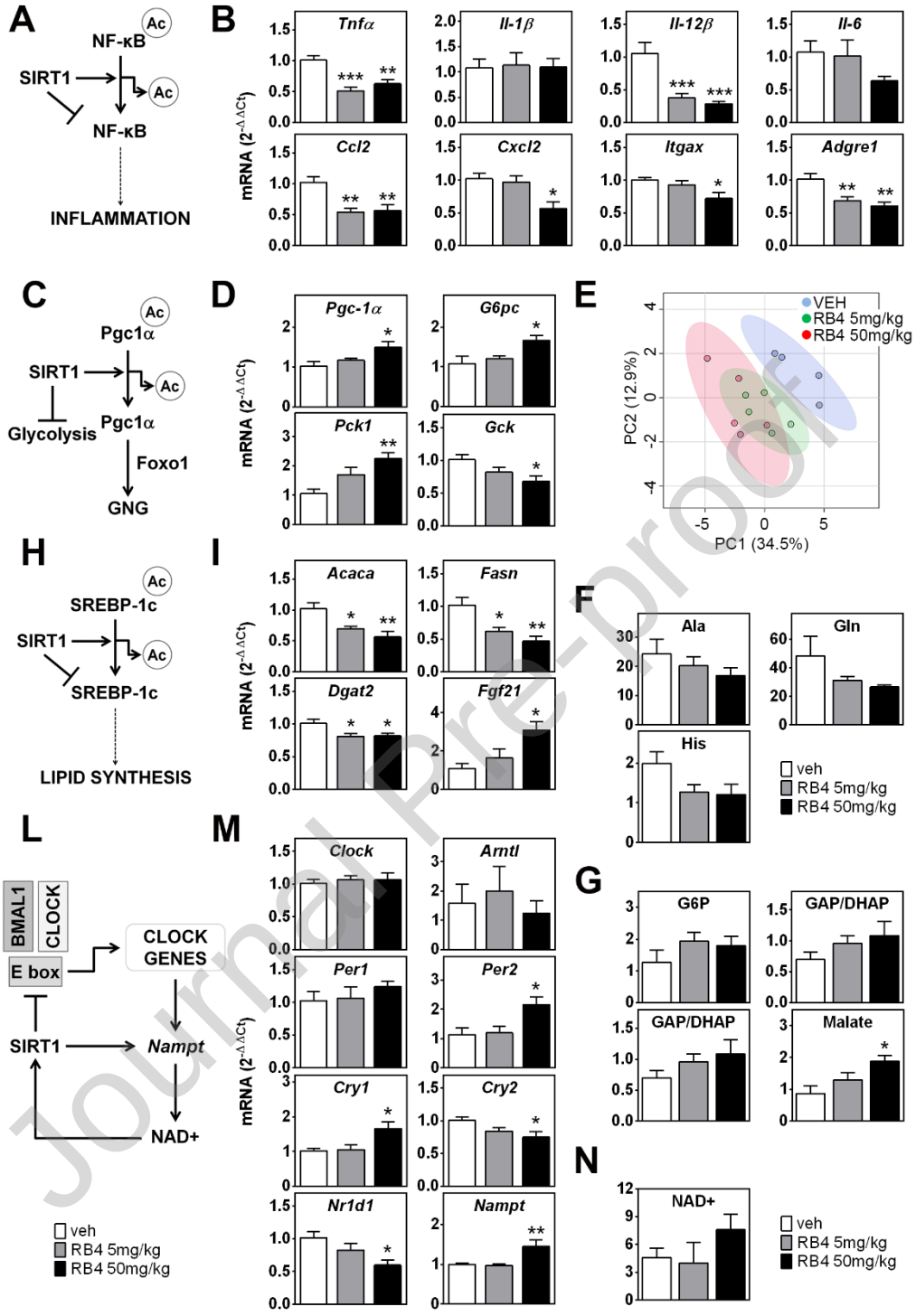

Figure 4: Liver transcriptomic and metabolomic analysis supports the *in vivo* Rb4-induced activation of SIRT1 signaling. Changes in the expression of genes and metabolites measured by rtPCR and MS in the liver in the liver of mice treated with vehicle (VEH), 5 mg/kg or 50 mg/kg RB4 for 3 days. **A**. Cartoon depicting the inhibitory regulation of inflammation signaling pathway as consequence of the SIRT1-mediated deacetylation of NF-κB (nuclear factor kappa B). **B**. mRNA content of well-known NF-κB target genes measured by rtPCR (n = 7). *Tnfα*, tumor necrosis factor α; *Il-1β*, interleukin 1 beta; *Il-12β*, interleukin 12 beta; *Il-6*, interleukin 6; *Ccl2*, C-C motif chemokine ligand 2 (Ccl2); *Cxcl2*, C-X-C motif chemokine ligand 2; *Itgax*,

integrin subunit alpha X; *Adgre1*, adhesion G protein-coupled receptor E1. **C**. Cartoon depicting the SIRT1-mediated regulation of glycolysis and gluconeogenesis (GNG) through the deacetylation of PGC-1α (PPARG coactivator 1 alpha). **D**. mRNA content of *Pgc-1α* and genes involved in glycolysis (*Gck*, glucokinase) and GNG (*G6pc*, glucose-6-phosphatase catalytic subunit; *Pck1*, phosphoenolpyruvate carboxykinase 1) measured by rtPCR. **E**. Score plot of PCA (Principal Component Analysis) of biologically relevant metabolites measured in the liver of mice treated with VEH or RB4. **F-G**. Liver content of some gluconeogenic amino acids (**F**) and of some metabolites metabolites belonging to Glyc/Gluc and TCA (**G**). **H**. Cartoon depicting the SIRT1-mediated regulation of lipogenesis through the deacetylation of SREBP-1c. **I**. mRNA content of genes involved in lipid synthesis (*Acaca*, acetyl-CoA carboxylase alpha; *Fasn*, fatty acid synthase; *Dgat2*, diacylglycerol O-acyltransferase 2) and of *Fgf21* (fibroblast growth factor 21) measured by rtPCR. **L**. Cartoon depicting the SIRT1-mediated regulation of clock genes. **M**. mRNA content of clock genes (*Clock*, clock circadian regulator; *Arntl*, aryl hydrocarbon receptor nuclear translocator like (*Bmal*); *Per1* and *Per2*, period circadian regulator 1 and 2; *Cry1* and *Cry2,* cryptochrome circadian regulator 1 and 2; *Nr1d1*, nuclear receptor subfamily 1 group D member 1) and *Nampt* (nicotinamide phosphoribosyltransferase) measured by rtPCR. **N**. Liver content of NAD^+. Data are presented as mean ± SEM. In (**B**, **D**, **I**, **M**), n=7; in (**F**, **G**, **N**), n=4. *p<0.05, **p<0.01 and ***p<0.001 *vs* VEH by one-way ANOVA followed by Bonferroni *post hoc* test.

DISCUSSION

In a prior study, we clarified the capacity of SIRT1 inhibitors characterized by an indene scaffold, such as exisulind, to snugly fit into the NAD^+ binding cleft adjacent to the STACs interaction domain that binds allosteric modulators of deacetylases. This discovery prompted us to synthesize and screen a variety of (*E*)-2'-des-methyl sulindac derivatives, with the goal of uncovering novel types of SIRT1 modulators. In this pursuit, we successfully discovered both SIRT1 inhibitors and activators. Notably, two of these derivatives (RB4 and RB7) exhibited a unique ability to activate SIRT1 in a dose-dependent manner, even in the absence of NAD^+. This suggests that NAD^+ might not be essential for their mechanism of action (Fig. 1E-F and 1L-M).

Based on these experimental data, and having also excluded that SIRT1 itself may fulfil the role of acetyl acceptor in the absence of NAD^+, it is likely that RB4 and RB7 participate in the deacetylation reaction. However, if we refer to the known mechanism of acetyl transfer from the donor acetylated

Lys to the acceptor NAD^+ [11,39], in contrast to NAD^+, RB4 does not possess any group that could serve as a leaving group in a nucleophilic substitution reaction, mimicking the nicotinamide portion.

On the other hand, our mass analysis of the biochemical reaction *in vitro* clearly showed the addition of a carboxymethyl radical, likely deriving from the acetylated peptide, to the molecule of RB-4. Similar behavior has been observed also for RB7 (See Supplementary Fig. 5). This insight received further support from our MS tracing of the acetyl moiety within the intact cellular context, using [U-$^{13}C_2$]-acetate. In this case MS analysis showed a parent ion peak (m/z 415), 2 Dalton higher in respect with the previous experiment.

Thus, further investigation is needed to shed light on the exact role played by RB4 and RB7 in the deacetylation reaction.

For some compounds, a non-canonical mechanism for Sirtuin activation has been recently proposed [40,41], indicating that some additional features in Sirtuin enzymatic activity may require additional attention from researchers in this field.

It remains that RB4 and RB7 constitute a new category of STACs with a distinct mechanism of action compared to previously identified SIRT1 activators. To our knowledge, these are the only STACs that do not require the presence of the cofactor as an acceptor molecule in the deacetylase reaction.

Although our experiments have not completely defined the exact biochemical mechanism of this enzymatic reaction, the docking poses align RB4 and RB7 within the NAD^+ binding cleft of the enzyme. In these poses, the acetyl-lysine of the substrate significantly bumps the biphenyl group of RB4 and the 1-naphthyl group of RB7.

Future investigations will focus on characterizing the biochemical process leading to the creation of acetyl derivatives, a crucial knowledge for designing a family of molecules based on RB4/RB7 leads, with potential for novel therapeutics.

This newly discovered family of STACs displays appealing pharmacological attributes. Our experiments in the cellular model suggest that the substituent in RB4 confers a better ability to activate the SIRT1 enzyme compared to RB7. This is why we have focused our investigation on RB4 for its in vivo ability to modulate key signaling pathways governed by this deacetylase. It is crucial to emphasize that the NAD^+-independent activity of exisulind derivatives on SIRT1 separates enzymatic activity from intracellular NAD^+ levels. NAD^+ plays a pivotal role as a metabolic sensor, influencing cellular bioenergetics, genomic stability, mitochondrial equilibrium, adaptive stress responses, and cell survival. NAD^+ serves as a cofactor for numerous key enzymes, including relevant sirtuins involved in these biological processes. The limitation of current STACs, acting as allosteric ligands that they require NAD^+ as an acetyl acceptor molecule due to their mechanism, is their reduced effectiveness when intracellular NAD^+ levels decline, as seen in the elderly and individuals with chronic illnesses like metabolic disorders, heart disease, and neurodegenerative conditions. This limitation can be addressed by compounds like RB4, offering an alternative strategy to NAD^+ boosting agents. These compounds might be developed to have more specific effects on sirtuins compared to the NAD^+ boosting agents, thus avoiding compensatory metabolic effects that limit efficacy [42,43] or side effects associated with prostaglandin activation [44] that were associated with these agents.

Significantly, our gene expression and metabolomics data support the effectiveness of RB4 as NAD^+-independent activators of the SIRT1 pathway in physiology. As a proof-of-concept, we indeed administered RB4 orally to male mice at two doses (5 and 50 mg/kg/day) over 3 days (Supplementary Fig. 6A). Focusing on the hepatic tissue, a key metabolic organ, and a known SIRT1 target [32,45], we tested the potential SIRT1 activation by RB4 by measuring the expression of well-established SIRT1 target genes *via* RT-PCR. We confirmed that RB4 treatment dose-dependently modulated main SIRT1 target pathways, including anti-inflammatory and those involved in the hepatic metabolism. Metabolomic analysis supported these gene expression findings, revealing the expected effects on

gluconeogenesis [33], lipid metabolism [34], and circadian regulation [36]. Importantly, RB4 treatment did not alter physiological parameters like food intake or body weight, which might interfere with the interpretation of our data, and histopathology did not uncover any significant side effects associated with acute treatment. However, a comprehensive toxicological analysis including repeated dose toxicity study should be conducted in the future to further investigate the safety of this compound class. Notably, histopathology supported RB4's potential anti-inflammatory activity by showing reduced neutrophil infiltration in the liver. Overall, the combined anti-inflammatory and metabolic effects observed in this short-term treatment highlight RB4's effectiveness in SIRT1 activation and its potential beneficial activity through the modulation of NAD^+-controlled pathways.

The (*E*)-2'-des-methyl sulindac derivatives selected for our studies exhibit weak or negligible COX-1 inhibitory activity and no COX-2 inhibitory activity [26,28]. However, it's worth noting that we cannot dismiss the possibility of additional activities on other targets. For example, these compounds have been reported to interact with PPARγ (peroxisome proliferator activated receptor gamma) *in vitro* and in cell lines. Notably, RB4 has shown the ability to enhance PPRE-mediated transcription, as demonstrated in a reporter assay [29]. The SIRT1 and PPARγ pathways are interconnected, sometimes cooperating in specific tissues and antagonizing in others. The NAD^+-independent activation of SIRT1 that we observed for RB4 aligns with the effects observed *in vivo* in the livers of mice treated with this compound. Specifically, RB4 decreased *Gck* levels and increased the expression of genes associated with lipid biosynthesis [46]. These findings are more consistent with SIRT1 activation and are not typically expected from PPARγ activation. Thus, it is reasonable to assert that the effects observed with RB4 treatment *in vivo* are primarily attributable to SIRT1 activation rather than PPARγ activation. Future studies should focus on elucidating and identifying more selective and potent SIRT1 activating compounds from the leads described in our study. Additionally, these studies should address critical factors such as pharmacokinetics, pharmacodynamics, and safety aspects essential for potential clinical translation. To this aim, it is important to note that the scaffold of this molecule has

been extensively studied in the past [26,27,29] and serves as the foundation for approved drugs like exisulind.

In conclusion, RB4 represents the first NAD^+-independent SIRT1 activator in the deacetylase activation reaction. We believe this molecule could serve as a lead compound to create a novel family of molecules with an intriguing action profile that mimics the physiological fed state. Such compounds hold significant potential for pharmacological applications in the prevention or treatment of metabolic diseases and age-related disorders.

MATERIAL & METHODS

Materials

Sodium acetate-$^{13}C_2$ (Sigma-Aldrich 282014).

The compounds under study RB2, RB4, RB7 and RB12, were prepared according to the procedure reported in the literature [29]. Reagents and solvents were purchased from Sigma-Aldrich or TCI Europe. The purity of the investigated compounds is ≥ 95%. ^{1}H NMR spectra are consistent with those reported in the literature [29].

SIRT1 enzymatic activity assay

SIRT1 enzymatic activity was measured with appropriate kit according to the manufacturer's protocol (Abcam, ab156065).

Cell culture

MDA-MB-231 were purchased from the American Type Culture Collection (ATCC) and grown in RPMI 1640 medium (Life Technology) supplemented with 10% FBS (Sigma-Aldrich) and streptomycinpenicillin (50,000 IU plus 50 mg/l). Cells were treated with RB4, RB7, exisulind, NAD^+ and DMSO as vehicle; compounds were appropriately diluted before treatment with cell culture

medium from a stock of 27mM dissolved in DMSO (Sigma Aldrich). For labeling experiment, cells were treated with 2mM 99 atom % [U-$^{13}C_2$]-acetate (Sigma Aldrich) 24 hours before lysate preparation.

Human HEK-293 cells and the corresponding line of human SIRT1-Knock out HEK-293 cells (AbCam) were purchased by Abcam who obtained the latter by Crispr/Cas9-mediated deletion of 19 bp validated by Next Generation sequencing. Cells were grown accordingly to manufacturer instruction in DMEM (high glucose) + 10% FBS.

Protein extracts and western blot analysis

Protein extracts were obtained by suspending pellet of cells in lysis buffer (10mM Tris-HCl, pH 7.4, 150mM NaCl, 15% glycerol, 1% Triton-X-100, 1mM sodium orthovanadate, 10 µg/ml leupeptin, 10 µg/ml aprotinin, 1mM NaF, protease inhibitor cocktail and 1mM PMSF), disrupting cell membranes by freezing and thawing and collecting supernatant after 35 min minifuge centrifugation at the maximal speed. 20 µg of protein extracts were separated in a PAGE and immunoblot assays were carried out using specific antibodies recognizing acetylated p53 (K382 residue, Cell Signalling Technology, 2525S) or total p53 (Pantropic Calbiochem, PC35) and anti-β-actin (Sigma, A1978). Immunoreactivity was detected with an ECL Western Blotting Analysis System (Amersham, GE Healthcare, RPN2109) and acquired and analyzed using an Odissey Fc Imaging system and the Image Studio™ software (LiCor Biosciences).

Sodium Acetate -$^{13}C_2$ labeling

MDAMB231 cells were seeded into 10 cm dish and cultured for 24 hours. The media were then replaced with labeling medium (RPMI 1640 supplemented with [U-$^{13}C_2$]-acetate) for 24 hours before protein extraction. Cells were washed twice with PBS and then lysed as described above. At 20 µg of protein lysate from control or labeled cells were added 5 µl of buffer 10x (SIRT1 Activity Assay Kit, ab156065) and RB4 2.7 mM and they react for 30 min at RT before mass spectrometry analysis.

Mass spectrometry analysis

50 µl of SIRT1 enzymatic assay or MDA-MB-231 cell lysate were diluted to 1ml or 500 µl with methanol, respectively. 200 µl of each sample were then infused and analyzed by negative ion mode ESI-IT-MS/MS (LTQ; Thermo Scientific). Collision energy up to 35 eV was used to detect the parent ion and product ions. Several transitions corresponding to isotopomers distribution were monitored.

Docking/ Molecular modelling procedures

Among all the solved structures of human SIRT1 the 4ZZI [17] PDB file was downloaded from the RCSB Protein Data Bank. All the crystallographic issues were fixed using the MOE Structure Preparation module. Structure was then submitted to an energy minimization step with the Amber10:EHT force field and the reaction field solvation model. The binding site of the selected protein was identified by the co-crystallized SIRT-1 inhibitor [47]. RB4 and RB7 were drawn by the MOE Builder and energy minimized by the MOE Energy Minimize program, down to an RMS gradient of 0.05 kcal/mol/Å2. Molecular docking was carried out through the MOE Dock program. The Triangle Matcher placement algorithm was selected, and the London dG empirical scoring function was used for sorting the poses. The 30 top-scoring poses were refined through molecular mechanics, considering each receptor as a rigid body, and the refined complexes were scored through the GBVI/WSA dG empirical scoring function, selecting the five top-scoring poses and estimating their binding free energy (ΔG) to the ligand- binding domain of the selected proteins. All the computational procedures have been carried out by the Molecular Operating Environment (MOE) version 2019.0102 [https://www.chemcomp.com], using the Amber10:EHT force field, as previously described [48].

Animals

In the present study, we used h C57BL/6J male mice 8 months of age. Mice were fed *ad libitum* with a maintenance, standard diet (SSNIFF, R/M-H V1534-300) and provided with filtered water. The animal room was maintained within a temperature range of 22–25 C, relative humidity of 50 ± 10%, and under an automatic cycle of 12-h light, 12-h dark (lights on at 7.00 am). All animal experimentation was performed in accordance with the ARRIVE guidelines and the European guidelines for animal care and the use of experimental animals, approved by the Italian Ministry of Research and University, and controlled by a departmental panel of experts. The animal study protocol was approved by "Istituto Superiore di Sanità - Ministero della Salute Italiano" under the agreement 611/2015 PR.

Animals were assigned to a specific experimental group and treated *per os* (gavage) for 3 days with vehicle or RB4 (5 and 50 mg/kg/day). RB4 was dissolved in dimethylsulfoxide (DMSO) and subsequently diluted in vehicle (2% Tween 80 and 0.5% carboxymethylcellulose water solution). Controls were treated with vehicle. Compounds were administered always at 9.00 am. At day 3, mice were sacrificed 6 hrs after the last treatment and under fasting conditions to keep low any possible confounding effect due to the circadian rhythm or feeding status. The tissues were explanted and fixed for histopathological analysis or frozen for total RNA extraction and metabolomics analysis.

Liver histopathology

Liver was sampled, fixed in 10% neutral buffered formalin and routinely processes for paraffin embedding. 4 µm thick sections were stained with Hematoxylin-Eosin and evaluated under a light microscope. A veterinary pathologist blinded to treatment groups, performed the assessments.

Real-Time PCR Gene Expression Analysis

Total liver RNA extraction was isolated with TRIzol Reagent (Invitrogen, #15596026) and purified using the Rneasy minikit protocol (Qiagen, #74034), according to the manufacturer's instructions.

For the preparation of cDNA, 1 µg RNA was denatured at 75°C for 5 min in the presence of 1.5 µg of random primers (Promega, #C1181) in 15 µl final volume. Deoxynucleotide triphosphate (GE Healthcare, #GEH28406552) and Moloney murine leukemia virus reverse transcriptase (M-MLV RT) (Promega, #M3682) were added at 0.5 mm and 8 U/µl final concentration, respectively, in a final volume of 25 µl. The RT reaction was performed at 37°C for 1 h; the enzyme was inactivated at 75°C for 5 min. Control reactions without addition of the RT enzyme were performed for each sample. For the real-time PCR experiments, the reaction mix for each sample was made up of 2 µl of pre-diluted cDNA, 5 µl of TaqMan 2× Universal PCR Master Mix No AmpErase UNG (ThermoFisher/Life Technologies, #4324018), 0.5 µl of 20x primers/probes mix, and 2.5 µl of H_2O. The primers used for the rtPCR reactions were listed in Supplementary Table 1. The 36b4 primer was used as reference gene assay. The reaction was carried out according to the manufacturer's protocol using QuantStudio™ 3 Real-Time PCR System with the following thermal profile: 2 min at 50°C; 10 min 95°C; 40 cycles (15 sec 95°C, 1 min at 60°C), and data were analyzed using the $2^{-\Delta\Delta Ct}$ method [49].

Metabolomic Analysis

For metabolomic analyses, liver tissues were homogenized with a tissue lyser. Briefly, tissues were lysed in 250 µl of methanol/acetonitrile 1:1 (v/v) with D-Glucose-$^{13}C_6$ 1 ng/µl (internal standard, Sigma Aldrich, 389374) and centrifuged at 4°C. Supernatant was saved for subsequent analysis. Amino acids quantification was performed through previous derivatization. Samples were incubated with PITC solution for 20 min at RT, dried and resuspended in 5 mM ammonium acetate in MeOH/H2O 1:1 (v/v). Metabolomic data were performed on an API-4000 triple quadrupole mass spectrometer (AB SCIEX) coupled with a HPLC system (Agilent) and CTC PAL HTS autosampler (PAL System). The identity of all metabolites was confirmed using pure standards. Quantification of different metabolites was performed with a liquid chromatography/tandem mass spectrometry (LC-MS/MS) method using a C18 column (Biocrates) for amino acids and cyano-phase LUNA column (50 mm x 4.6 mm, 5 µm; Phenomenex). AA were analyzed through a 10 min run in positive while

other metabolites were run in negative ion mode in a 5 min. run. 20 of multiple reaction monitoring (MRM) transition in positive ion mode (AA) and 30 MRM transition in negative ion mode (all other metabolites) were selected, respectively. The mobile phases for positive ion mode analysis (AA) were phase A: 0.2% formic acid in water and phase B: 0.2% formic acid in acetonitrile. The gradient was T_0 100% A, $T_{5.5}$min 5%A, T_7min 100%A with a flow rate of 500 µl/min. The mobile phase for negative ion mode analysis (all other metabolites) was phase A: 5 mM ammonium acetate pH 7.00 in MeOH. The gradient was 100% A for all the analysis with a flow rate of 500 µl/min. MultiQuant™ software (version 3.0.2) was used for data analysis and peak review of chromatograms. Quantitative evaluation of all metabolites was performed based on calibration curves with pure standards, then data were normalized on micrograms of proteins. Metabolomic data analysis was performed by using Metaboanalyst 3.0 software (http://www.metaboanalyst.ca/).

Quantification and statistical analysis

Statistical analyses were performed by Student's *t-test* for the comparison of two different experimental groups, or one-way ANOVA followed by Bonferroni's *post hoc* test for multiple testing comparisons. All statistical analyses were performed using GraphPad Prism 5.0 (GraphPad Software). All data are expressed as mean ± SEM. A p value less than 0.05 was considered statistically significant. The statistical parameters can be found in the figure legends.

Acknowledgements: We are grateful to Francesca Stucchi, Clara Meda and Monica Rebecchi for technical assistance. This work was mainly supported by AIRC under IG 2020 -ID.24914 project (P.C.), European Union—NextGenerationEU (PNRR M4C2-Investimento 1.4-CN00000041-23 PNRR_CN3RNA_SPOKE9) to P.C. This work was partially supported by the Ministry of University and Research (MUR) Progetto Eccellenza (2023–2027) to the Department of Pharmacological and Biomolecular Sciences "Rodolfo Paoletti", Università degli Studi di Milano and partially by the Italian Ministry of Health with Ricerca Corrente and "5xmille" funds to N.M. L.P. has been supported

by Linea 2 - Azione A 2022. LP, IE, NM have been supported by MIUR-Progetto di Eccellenza 2022-2025.

Conflict of interest: The authors declare that they have no conflict of interest.

Author contributions: Conceptualization: A.P, P.Co., P.Ci.; Methodology: P.Ci., I.E., N.M., P.Co.; Investigation: G.D., J.D., L.P., E.S., N.M., A.V., S.D.T., P.Co., I.E., A.P.; Writing – Original Draft: S.D.T., A.V. and P.Ci.; Writing - Review and editing: all authors; Resources: P.Ci., E.S., P.Co., I.E., N.M.; Funding acquisition: P.Ci., N.M., L.P., I.E.; Supervision: P.Ci.
All authors have read and agreed to the published version of the manuscript.

References

1. Chew, N. W. S. *et al.* The global burden of metabolic disease: Data from 2000 to 2019. *Cell Metabolism* **35**, 414-428.e3 (2023).
2. Amorim, J. A. *et al.* Mitochondrial and metabolic dysfunction in ageing and age-related diseases. *Nat Rev Endocrinol* **18**, 243–258 (2022).
3. Guo, J. *et al.* Aging and aging-related diseases: from molecular mechanisms to interventions and treatments. *Signal Transduct Target Ther* **7**, 391 (2022).
4. Hodes, R. J. *et al.* Disease drivers of aging. *Annals of the New York Academy of Sciences* **1386**, 45–68 (2016).
5. Franceschi, C., Garagnani, P., Parini, P., Giuliani, C. & Santoro, A. Inflammaging: a new immune–metabolic viewpoint for age-related diseases. *Nat Rev Endocrinol* **14**, 576–590 (2018).
6. Kubben, N. & Misteli, T. Shared molecular and cellular mechanisms of premature ageing and ageing-associated diseases. *Nat Rev Mol Cell Biol* **18**, 595–609 (2017).

7. Imai, S. & Guarente, L. NAD+ and sirtuins in aging and disease. *Trends in Cell Biology* **24**, 464–471 (2014).

8. Houtkooper, R. H., Pirinen, E. & Auwerx, J. Sirtuins as regulators of metabolism and healthspan. *Nat Rev Mol Cell Biol* **13**, 225–238 (2012).

9. Wu, Q.-J. *et al.* The sirtuin family in health and disease. *Signal Transduct Target Ther* **7**, 402 (2022).

10. Morris, B. J. Seven sirtuins for seven deadly diseases ofaging. *Free Radical Biology and Medicine* **56**, 133–171 (2013).

11. Imai, S., Armstrong, C. M., Kaeberlein, M. & Guarente, L. Transcriptional silencing and longevity protein Sir2 is an NAD-dependent histone deacetylase. *Nature* **403**, 795–800 (2000).

12. Sauve, A. A. Sirtuin chemical mechanisms. *Biochimica et Biophysica Acta (BBA) - Proteins and Proteomics* **1804**, 1591–1603 (2010).

13. Bordone, L. *et al.* SIRT1 transgenic mice show phenotypes resembling calorie restriction. *Aging Cell* **6**, 759–767 (2007).

14. Mitchell, S. J. *et al.* The SIRT1 Activator SRT1720 Extends Lifespan and Improves Health of Mice Fed a Standard Diet. *Cell Reports* **6**, 836–843 (2014).

15. Howitz, K. T. *et al.* Small molecule activators of sirtuins extend Saccharomyces cerevisiae lifespan. *Nature* **425**, 191–196 (2003).

16. Hubbard, B. P. & Sinclair, D. A. Small molecule SIRT1 activators for the treatment of aging and age-related diseases. *Trends in Pharmacological Sciences* **35**, 146–154 (2014).

17. Dai, H. *et al.* Crystallographic structure of a small molecule SIRT1 activator-enzyme complex. *Nat Commun* **6**, 7645 (2015).

18. Gertz, M. *et al.* A Molecular Mechanism for Direct Sirtuin Activation by Resveratrol. *PLOS ONE* **7**, e49761 (2012).

19. Dai, H. *et al.* SIRT1 Activation by Small Molecules. *Journal of Biological Chemistry* **285**, 32695–32703 (2010).

20. Borra, M. T., Smith, B. C. & Denu, J. M. Mechanism of Human SIRT1 Activation by Resveratrol. *Journal of Biological Chemistry* **280**, 17187–17195 (2005).

21. Kaeberlein, M. *et al.* Substrate-specific Activation of Sirtuins by Resveratrol. *Journal of Biological Chemistry* **280**, 17038–17045 (2005).

22. Pacholec, M. *et al.* SRT1720, SRT2183, SRT1460, and Resveratrol Are Not Direct Activators of SIRT1. *Journal of Biological Chemistry* **285**, 8340–8351 (2010).

23. Cao, D. *et al.* Structural basis for allosteric, substrate-dependent stimulation of SIRT1 activity by resveratrol. *Genes Dev.* **29**, 1316–1325 (2015).

24. Rajman, L., Chwalek, K. & Sinclair, D. A. Therapeutic Potential of NAD-Boosting Molecules: The In Vivo Evidence. *Cell Metab* **27**, 529–547 (2018).

25. Dell'Omo, G. *et al.* Inhibition of SIRT1 deacetylase and p53 activation uncouples the anti-inflammatory and chemopreventive actions of NSAIDs. *Br J Cancer* **120**, 537–546 (2019).

26. Liedtke, A. J. *et al.* Cyclooxygenase-1-Selective Inhibitors Based on the (*E*)-2′- *Des* -methyl-sulindac Sulfide Scaffold. *J. Med. Chem.* **55**, 2287–2300 (2012).

27. Walters, M. J. *et al.* The influence of double bond geometry in the inhibition of cyclooxygenases by sulindac derivatives. *Bioorganic & Medicinal Chemistry Letters* **19**, 3271–3274 (2009).

28. Felts, A. S. *et al.* Desmethyl Derivatives of Indomethacin and Sulindac as Probes for Cyclooxygenase-Dependent Biology. *ACS Chem. Biol.* **2**, 479–483 (2007).

29. Felts, A. S. *et al.* Sulindac Derivatives That Activate the Peroxisome Proliferator-activated Receptor γ but Lack Cyclooxygenase Inhibition. *J. Med. Chem.* **51**, 4911–4919 (2008).

30. Beher, D. *et al.* Resveratrol is Not a Direct Activator of SIRT1 Enzyme Activity. *Chem Biol Drug Des* **74**, 619–624 (2009).

31. Solomon, J. M. *et al.* Inhibition of SIRT1 Catalytic Activity Increases p53 Acetylation but Does Not Alter Cell Survival following DNA Damage. *Molecular and Cellular Biology* **26**, 28–38 (2006).

32. Chang, H.-C. & Guarente, L. SIRT1 and other sirtuins in metabolism. *Trends in Endocrinology & Metabolism* **25**, 138–145 (2014).

33. Yang, T., Fu, M., Pestell, R. & Sauve, A. A. SIRT1 and endocrine signaling. *Trends in Endocrinology & Metabolism* **17**, 186–191 (2006).

34. Wang, L.-F. *et al.* Inhibition of NAMPT aggravates high fat diet-induced hepatic steatosis in mice through regulating Sirt1/AMPKα/SREBP1 signaling pathway. *Lipids Health Dis* **16**, 82 (2017).

35. Li, Y. *et al.* Hepatic SIRT1 Attenuates Hepatic Steatosis and Controls Energy Balance in Mice by Inducing Fibroblast Growth Factor 21. *Gastroenterology* **146**, 539-549.e7 (2014).

36. Nakahata, Y. *et al.* The NAD+-Dependent Deacetylase SIRT1 Modulates CLOCK-Mediated Chromatin Remodeling and Circadian Control. *Cell* **134**, 329–340 (2008).

37. Ramsey, K. M. *et al.* Circadian Clock Feedback Cycle Through NAMPT-Mediated NAD^+ Biosynthesis. *Science* **324**, 651–654 (2009).

38. Garten, A. *et al.* Physiological and pathophysiological roles of NAMPT and NAD metabolism. *Nat Rev Endocrinol* **11**, 535–546 (2015).

39. Feldman, J. L., Dittenhafer-Reed, K. E. & Denu, J. M. Sirtuin catalysis and regulation. *J Biol Chem* **287**, 42419–42427 (2012).

40. Yu, N.-D., Wang, B., Li, X.-Z., Han, H.-Z. & Liu, D. A Novel Mechanism for SIRT1 Activators That Does Not Rely on the Chemical Moiety Immediately C-Terminal to the Acetyl-Lysine of the Substrate. *Molecules* **27**, 2714 (2022).

41. Suenkel, B. *et al.* Potent and Specific Activators for Mitochondrial Sirtuins Sirt3 and Sirt5. *J Med Chem* **65**, 14015–14031 (2022).

42. Kang-Lee, Y. A. *et al.* Metabolic Effects of Nicotinamide Administration in Rats. *The Journal of Nutrition* **113**, 215–221 (1983).

43. Gale, E. a. M., Bingley, P. J., Emmett, C. L., Collier, T., & European Nicotinamide Diabetes Intervention Trial (ENDIT) Group. European Nicotinamide Diabetes Intervention Trial (ENDIT): a randomised controlled trial of intervention before the onset of type 1 diabetes. *Lancet* **363**, 925–931 (2004).

44. Puhl, A. C. *et al.* Mechanisms of Peroxisome Proliferator Activated Receptor γ Regulation by Non-steroidal Anti-inflammatory Drugs. *Nucl Recept Signal* **13**, nrs.13004 (2015).

45. Rui, L. Energy Metabolism in the Liver. in *Comprehensive Physiology* (ed. Terjung, R.) 177–197 (Wiley, 2014). doi:10.1002/cphy.c130024.

46. Kraakman, M. J. *et al.* PPARγ deacetylation dissociates thiazolidinedione's metabolic benefits from its adverse effects. *Journal of Clinical Investigation* **128**, 2600–2612 (2018).

47. Zhao, X. *et al.* The 2.5 Å Crystal Structure of the SIRT1 Catalytic Domain Bound to Nicotinamide Adenine Dinucleotide (NAD^+) and an Indole (EX527 Analogue) Reveals a Novel Mechanism of Histone Deacetylase Inhibition. *J. Med. Chem.* **56**, 963–969 (2013).

48. Lauria, S. *et al.* Design, synthesis, molecular modelling and in vitro cytotoxicity analysis of novel carbamate derivatives as inhibitors of Monoacylglycerol lipase. *Bioorganic & Medicinal Chemistry* **26**, 2561–2572 (2018).

49. Schmittgen, T. D. & Livak, K. J. Analyzing real-time PCR data by the comparative CT method. *Nat Protoc* **3**, 1101–1108 (2008).

Graphical abstract

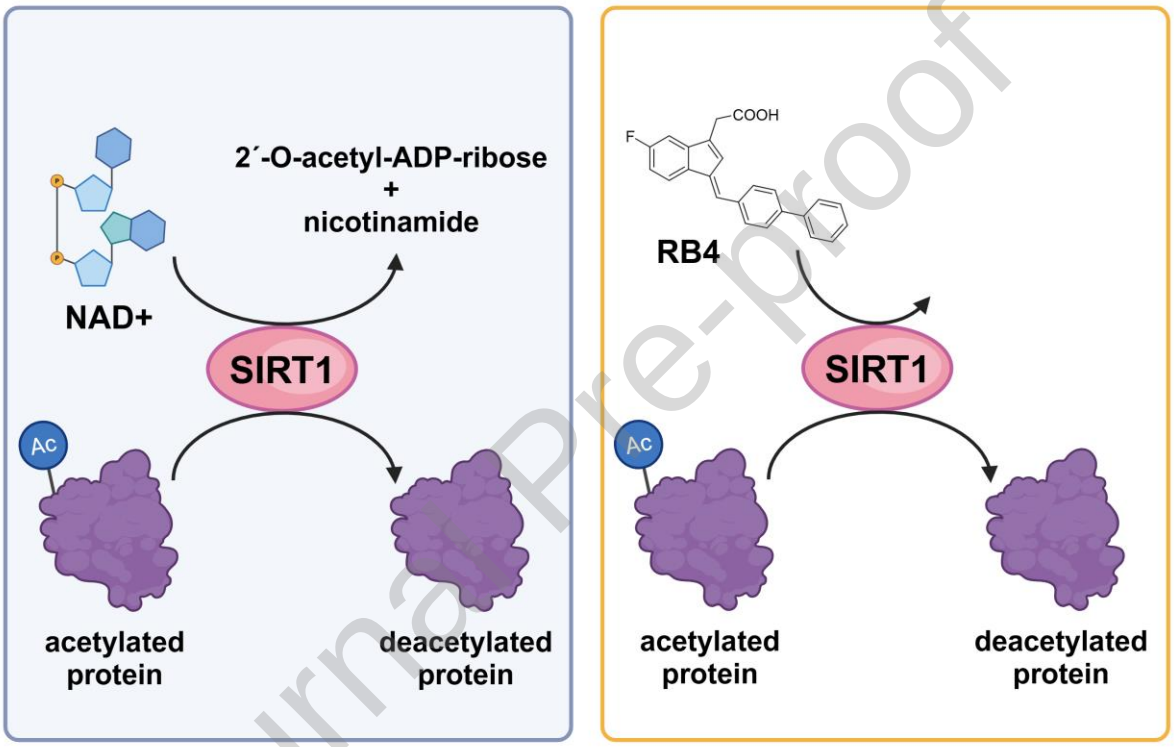

Declaration of interest

The authors declare that they have no conflict of interest.